Numerical Simulation: Field Scale Fluid Injection to a Porous Layer in relevance to CO_2 Geological Storage

Seunghee Kim[*1], Seyyed A. Hosseini[1], and Susan D. Hovorka[1]
[1]Bureau of Economic Geology, Jackson School of Geosciences, University of Texas at Austin
*Corresponding author: 10100 Burnet Rd, bldg.130, Austin, TX 78758, USA, simseung@gmail.com

Abstract: CO_2 geological storage can help to provide a "bridge" from a fossil-fuel dependent system to a more diversified energy portfolio. Pressure monitoring for an injection zone (IZ) and an above-zone monitoring interval (AZMI) has been under operation at a field-scale CO_2 injection site, Cranfield, MS. Recorded pressure data in the AZMI revealed a certain amount of increase with no evidence of direct fluid flow between the IZ and the AZMI. We therefore attempted to interpret the field-measurement data from a geomechanical perspective. We conducted numerical simulations in which fully coupled calculation between fluid flow and geomechanics was implemented. Numerical-simulation results using COMSOL matched well with the field-measurement data obtained from the AZMI.

Keywords: CO_2 geological storage, above-zone pressure monitoring, poroelasticity, COMSOL.

1. Introduction

Burning of fossil fuels, and, thus, emission of carbon dioxide and other greenhouse gases to the atmosphere has been referred to as a main culprit in global warming. Coal and natural-gas power plants account for more than one-third of total carbon emissions worldwide (IPCC, 2005). However, fossil-fuel-based power plants should probably not be abandoned immediately, given our dependence on them for electricity. For this reason, Regional Carbon Sequestration Partnerships (RCSP), which consist of seven major regional partnerships in the United States, have been conducting a number of small- and large-scale CO_2 injection projects to ensure the reliability of the carbon capture, utilization and storage (CCUS) and to raise it to an industrial scale (NETL, 2012). Cranfield pilot site, Mississippi, is one of the largest CO_2 injection projects; as of July 2013, about 4 million metric tons of CO_2 had been injected (Hovorka et al., 2013). Various monitoring strategies targeting different intervals, ranging from the injection to the vadose zones, have been utilized in monitoring migration of the CO_2 plume at the Cranfield test site. In particular, pressure and temperature monitoring of an above-zone monitoring interval (AZMI) has been attempted for the first time in CO_2-injection history (Hovorka et al., 2013). Increase in fluid pore pressure was thought to be minimal if no massive communication were to occur between an injection zone (IZ) and an AZMI. However, measured increase in AZMI pore pressure at Cranfield was not small enough to be neglected, even though no evidence of CO_2 leakage was found during the injection period (Meckel et al., 2013; Tao et al., 2012). Given this observation, we attempted to interpret measurement data from a geomechanical-response perspective.

2. Site Characteristics

The Cranfield site in southwestern Mississippi, USA, which comprises a near-circular, four-way anticline, was active from discovery in 1943 to 1966 (Hosseini et al., 2012). During an idle period between 1966 and 2008, reservoir pressure recovered close to initial value via the incursion of formation water (Hovorka et al., 2013), and CO_2 injection began in 2008 for enhanced oil recovery (EOR).

The Tuscaloosa Formation overlies shale and sandstones of the Washita-Fredericksburg Formations in the Cranfield site (Figure 1). The injection interval is the lower Tuscaloosa Formation, fluvial conglomerates and sandstones (D/E sand), that are located at a depth of 3,167 m (10,420 ft); interval thickness ranges from 14 to 24 m. Porosity and permeability show wide variability (maximum porosity is ~0.32, and gas permeability is as high as hundreds of millidarcys; Ajo-Franklin et al., 2013). The main constituent is quartz (~80%), followed by chlorite (~12%; dominant coating and pore-filling grains), iron-bearing dolomite, and calcite (Hosseini et al., 2012; Ajo-Franklin et al., 2013). Overlying the IZ is a sequence of mudstones and muddy sandstones that form the lower part of the

Cranfield confining system (Lu et al., 2011; Nicot et al., 2012). The upper Tuscaloosa Formation is a thin (10 to ~20 m), permeable interval that lies above the confining layers. This formation, ~3,060 m deep and located ~120 m above the injection interval, was chosen as the AZMI.

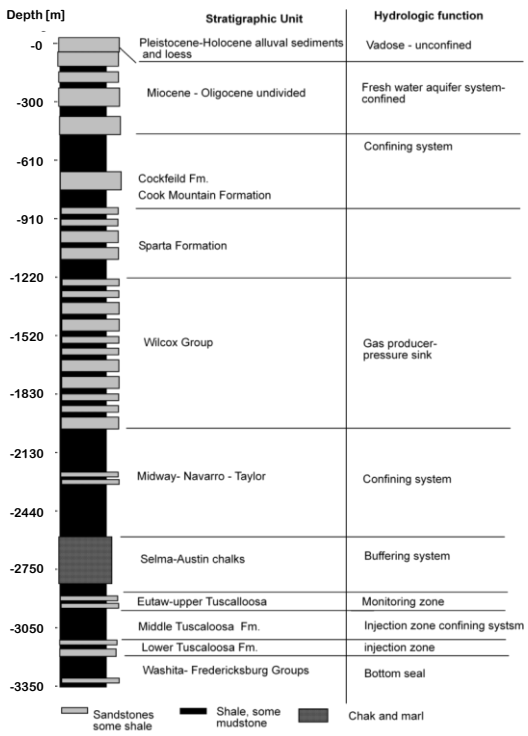

Figure 1. Stratigraphic section for Cranfield test site (modified from Hovorka et al., 2011). The injection interval selected for the test was the lower Tuscaloosa Formation. The regional confining zone overlying the injection interval is middle Tuscaloosa "marine" mudstone and associated low-permeability facies. Upper Tuscaloosa formation was selected for the above-zone monitoring interval. Overburden includes diverse units and isolates the injection zone from shallow gas resources (Wilcox group) and underground sources of drinking water (USDW), which occur at depths of 30 to 600 m below land surface.

CO_2 injection began in the study area on December 1, 2009. The initial injection rate, which was ~175 kg/min, doubled to ~330 kg/min on December 19, 2009. The injection rate was again increased to ~550 kg/min in May 2010. Injected CO_2 is colder than hot formation water; the difference recorded at the bottom hole of the injection well is ΔT=~44°C (initial temperature is 122~124°C; Hosseini et al., 2012). During CO_2 injection, pressure and temperature had been monitored at the bottom holes of the injection well and the observation well, located 110m far from the injection well, for both IZ and AZMI. The increase in fluid pore pressure in the AZMI was recorded at ~ΔP=40 kPa after ~7 months of CO_2 injection operation.

3. Use of COMSOL Multiphysics

3.1 Simulation Method

We used the commercial software COMSOL to numerically experiment fluid injection into a porous-medium underground. The subsurface-flow module in COMSOL contains predefined sets of equations adapted to many earth science applications (COMSOL, 2012). These equations include those for momentum transport (fluid flow), energy transport (heat transfer), and mass transport. The module also supplies predefined options for describing mass transfer by convection (advection), dispersion, diffusion, sorption, and reactions. In this module, a poroelasticity interface combines a transient formulation of Darcy's law with a geomechanics interface. Of the two major constitutive equations defining poroelastic behavior, Darcy's law describes the flow field in a poroelastic medium. The fluid equation comes from mass conservation:

$$\frac{\partial}{\partial t}(\rho_f \varphi) + \nabla \cdot (\rho_f u) = Q \qquad (1)$$

where ρ_f denotes density of fluid, φ porosity of the medium, and Q injection rate. Darcy's velocity u and the storage model are:

$$u = -\frac{k}{\eta}(\nabla p + \rho_f g \nabla h) \qquad (2)$$

$$\frac{\partial}{\partial t}(\rho_f \varphi) = \rho_f S \frac{\partial p}{\partial t} \qquad (3)$$

where k is permeability of an injection interval, η is viscosity of fluid, and p and h are pressure and elevation head, respectively. Storage coefficient S is a function of Biot coefficient α, fluid bulk-modulus K_f, and drained bulk-modulus K_d:

$$S = \frac{\varphi}{K_f} + (\alpha - \varphi)\frac{1-\alpha}{K_d} \qquad (4)$$

The other constitutive equation relates stress σ, strain ε, and fluid pore pressure p:

$$\bar{\sigma} = \bar{\bar{C}}\bar{\varepsilon} - \alpha p \bar{\bar{I}} \quad (5)$$

Elasticity matrix C in Equation 5 must be measured under a drained condition. I denotes identity matrix. If Equation 5 is divided into volumetric and deviatoric parts, the deviatoric part (shear stress) is independent of pore-pressure coupling. Coupling in the volumetric part can be written as:

$$\frac{\sigma_{kk}}{3} = K_d \varepsilon_{vol} - \alpha p \quad (6)$$

where σ_{kk} denotes mean stress and ε_{vol} represents volumetric strain. The governing equations are fully coupled during numerical simulation, and computation iterates between these equations for each time step within a finite-difference method.

3.2 Model and Boundary Conditions

We built the simulation model as simple as possible without losing geometric relevance to a field condition. The model retains an axisymmetric configuration in which the left side is a central axis (Figure 2). The AZMI is 120 m above the IZ, and these two intervals are the only layers with a high permeability value in the model. Other layers are assigned a low permeability value, k=1 nd (Table 1), so that the confining layer between the two permeable intervals acts as a hydraulic barrier. Thickness of the two intervals is identical, at 20 m. The right side of these two intervals is set at the fluid outlet. The top and bottom are set at the closed fluid boundary. In mechanical boundary conditions, a roller is imposed on the left and right sides and the bottom (i.e., perpendicular displacement is not allowed, whereas transitional displacement is allowed). The top surface is free to move. Radial and vertical boundaries are 10 km away from the left and 6 km away from the top, respectively, to avoid any boundary effect. A dot in the AZMI represents the location of monitoring point. Fluid injection, that is imposed on the left-end of the injection zone, is initially 175kg/min (0.1MtCO_2/yr) and doubles after 19days, and increases again to 500kg/min (0.3MtCO_2/yr) after 183 days. Total simulation time is about 230 days ($\approx 10^{7.3}$ seconds).

Table 1: Input parameters for numerical simulations

Parameters	Value	
	IZ & AZMI	Else
Young's modulus	17.5GPa	30GPa
Poisson's ratio	0.15	0.3
Drained bulk density	2650kg/m^3	2000kg/m^3
Porosity	0.25	0.1
Biot coefficient	1	1
Permeability	64md	1nd
Bulk modulus of fluid	2.2GPa	
Density of fluid	1000kg/m^3	
Viscosity of fluid	0.001Pa·s	
Injection rate	175→330→500kg/min	

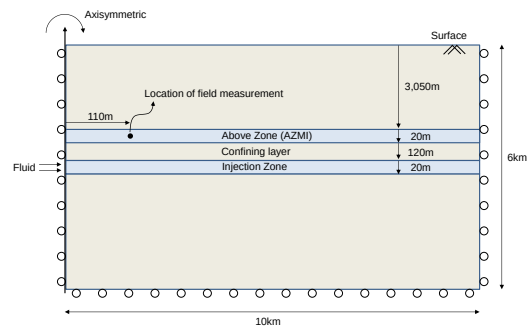

Figure 2. Simulation model and geometric conditions for numerical-experiments using COMSOL.

4. Result

Numerical simulation yields an ideal response to bottom-hole pressure increase near the injection well: bottom-hole pressure exhibits a sudden increase corresponding to the onset of injection and/or change in injection rate (Figure 3). However, this typical response is not observed in the field data (Figure 4). Pressure monitoring actually suggests that bottom-hole pressure spiked during early initial injection then decreased to some extent to level off at ΔP~6.21 MPa until an increase in injection rate from 175 to 330 kg/min (Figure 4). This behavior implies that the IZ may have experienced some reactivation of existing discontinuities or hydraulic fracturing near the injection well. The likelihood of these geomechanical failures is able

to explain the absence of another jump in bottom-hole pressure in the field data at ~180 days passed once injection began (Figures 4), as was suggested by Hosseini et al. (2012). Possible events of geomechanical failure might also explain the final increase in bottom-hole pressure being higher in the numerical-simulation results (ΔP~14 vs. ΔP~9 MPa; Figure 4).

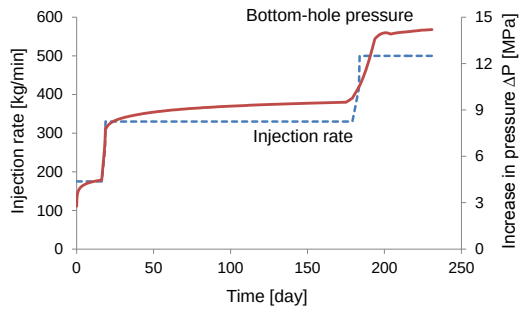

Figure 3. Numerical simulation results: Imposed injection rate (dotted line) and resulting bottom-hole pressure near the injection well (solid line).

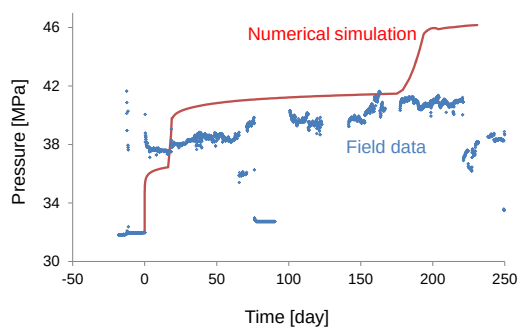

Figure 4. Injection-zone analysis: Comparison of bottom-hole pressure near injection well between field-measurement data and numerical simulation results.

When it comes to pressure increase in AZMI, field-measurement data and numerical-simulation results are in accordance, even if not totally consistent (Figure 5). Both graphs show in detail a jump immediately following CO_2 injection began (around zero time elapse) and exhibit another jump following increase in injection rate (~20 day time elapse). After the second jump, both graphs show relatively constant pressure. Absolute pore-pressure increase after ~230 days is also comparable (ΔP~40 kPa for both graphs).

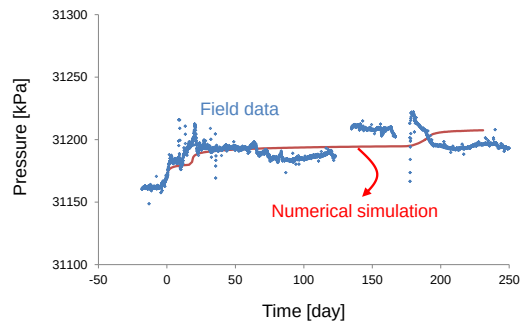

Figure 5. Comparison of bottom-hole pressure between field-measurement data (dots) and numerical simulation results (solid line) for AZMI.

We were also able to investigate probable displacements at the surface: maximum value reached ~1.2mm at the central point after 230days (Figure 6).

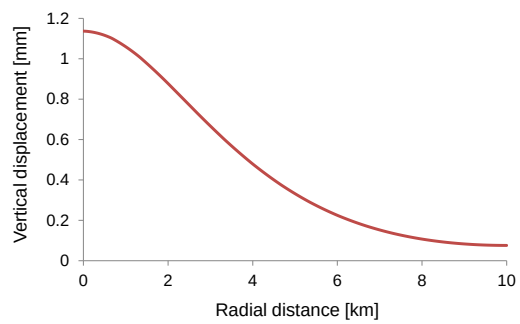

Figure 6. Distribution of vertical displacement at the surface, as a result of CO_2 injection.

Finally, coupling of pore pressure-stress was observed during the numerical simulations (Figure 7). Specifically, increase in pore pressure is linked to increase in total stress (also decrease in pore pressure is linked to decrease in total stress). This coupling is more pronounced for total horizontal stress because lateral deformation is isolated within sedimentary basins. A summary of reported field data from many oil-production sites suggests that this pore-pressure–total-horizontal-stress coupling ratio ranges to $0.46<\Delta\sigma_h/\Delta P<1.18$, depending on formation history and initial stress ratio (Addis, 1997; Hillis, 2000; Hillis, 2001). For an ideally thin, laterally extensive reservoir, the pore-pressure–horizontal-stress coupling ratio can be estimated on the basis of poroelasticity (Hawkes et al., 2005; Rutqvist et al., 2008):

$$\frac{\Delta\sigma_h}{\Delta P} = \alpha \frac{1-2\nu}{1-\nu} \quad (7)$$

For the simulation conditions in this study, the ratio of increase in total radial stress to increase in pore pressure was found to be similar to $\Delta\sigma_{rr}/\Delta P \approx 0.82$ (value calculated from α=1 and ν=0.15 in Equation 7) at the interface of the IZ and overlying confining layer (Figure 7). Note that the ratio of increase in total vertical stress to increase in pore pressure is not negligible ($\Delta\sigma_{zz}/\Delta P \approx 0.3$; Figure 7). Traditionally, total vertical stress has been supposed to be unaffected by changes in pore pressure because the upper boundary (i.e., surface) is free to move (Addis, 1997; Hillis, 2000; Hawkes et al., 2005). Therefore, accounting for the coupling between both horizontal & vertical stresses and pore pressure is needed on a site-specific basis to provide more realistic value of the pressure limit, which should be in conjunction with thermal consideration.

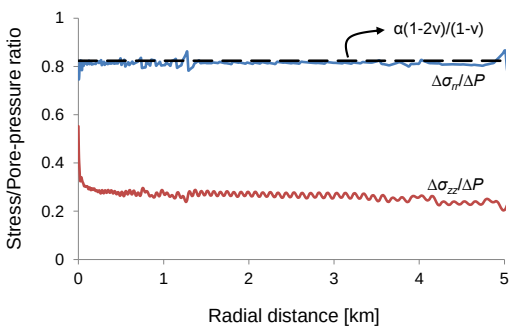

Figure 7. Pore-pressure/stress coupling: ratio of change in total radial stress to change in pore-pressure $\Delta\sigma_{rr}/\Delta P$ and ratio of change in total vertical stress to change in pore-pressure $\Delta\sigma_{zz}/\Delta P$. Note: dotted line represents theoretical ratio of change in total horizontal stress to change in pore-pressure $\Delta\sigma_h/\Delta P$, which is analogous to $\Delta\sigma_{rr}/\Delta P$, for the ideally thin, laterally extensive reservoir, given poroelasticity (α=1 and ν=0.15 for numerical simulations).

5. Conclusions

Numerical simulations using COMSOL for the fluid injection into a porous interval helped in interpreting the field observation: increase in pore pressure in the AZMI resulted from poroelastic effects, not from fluid leakage. Besides, we were able to obtain additional information such as displacements and pore pressure/stress coupling, which are valuable data for the risk assessment. This numerical-experiment technique can be utilized in various ways: (1) preliminary evaluation of geomechanical responses, (2) more reliable risk assessment of geomechanical failures, and (3) interpretation of field monitoring data.

6. References

1. IPCC, *IPCC special report on carbon dioxide capture and storage*, Cambridge, United Kingdom and New York, USA. Cambridge University Press (2005).
2. NETL, US DOE, *The United States 2012 Carbon Utilization and Storage ATLAS* - 4th edition (2012).
3. Hovorka, S.D., Meckel, T.A., and Treviño, R.H., Monitoring a large-volume injection at Cranfield, Mississippi - Project design and recommendations, *International Journal of Greenhouse Gas Control*, http://dx.doi.org/10.1016/j.ijggc.2013.1003.1021 (2013).
4. Meckel, T., Zeidouni, M., Hovorka, S.D., and Hosseini, S., Assesing sensitivity to well leakage from three years of continuous reservoir pressure monitoring during CO_2 injection at Cranfield, MS, *International Journal of Greenhouse Gas Control*,http://dx.doi.org/10.1016/j.ijggc.2013.1001.1019 (2013).
5. Tao, Q., Bryant, S.L., and Meckel, T., Modeling above-zone measurements of pressure and temperature for monitoring CCS sites, *International Journal of Greenhouse Gas Control*, http://dx.doi.org/10.1016/j.ijggc.2012.1008.1011 (2012).
6. Hosseini, S.A., Lashgari, H., Choi, J-W., Nicot, J-P., Lu, J., and Hovorka, S.D., Static and dynamic reservoir modeling for geological CO_2 sequestration at Cranfield, Mississippi, USA, *International Journal of Greenhouse Gas Control*, http://dx.doi.org/10.1016/j.ijggc.2012.1011.1009 (2012).
7. Ajo-Franklin, J.B., Peterson, J., Doetsch, J., and Daley, T.M., High-resolution characterization of a CO_2 plume using crosswell seismic tomography: Cranfield, MS, USA, *International Journal of Greenhouse Gas Control*,

http://dx.doi.org/10.1016/j.ijggc.2012.1012.1018 (2013).
8. Lu, J., Milliken, K., Reed, R.M., and Hovorka, S., Diagenesis and sealing capacity of the middle Tuscaloosa mudstone at the Cranfield carbon dioxide injection site, Mississippi, USA, *Environmental Geosciences*, 18(1), 35-53 (2011).
9. Nicot, J-P., Oldenburg, C.M., Houseworth, J.E., and Choi, J-W., Analysis of potential leakage pathways at the Cranfield, MS, USA, CO_2 sequestration site, *International Journal of Greenhouse Gas Control*, http://dx.doi.org/10.1016/j.ijggc.2012.1010.1011 (2012).
10. Hovorka, S., Clift, S.J., Meckel, T.A., Treviño, R.H., Zeng, H., Nicot, J-P. et al., Final Report for Gulf Coast Stacked-Storage Project SECARB Phase II at Cranfield, prepared for Southeast Regional Carbon Sequestration Partnership: Bureau of Economic Geology, The University of Texas at Austin (2011).
11. COMSOL, *4.3 User's Guide*. COMSOL Multiphysics (2012).
12. Addis, M., The stress-depletion response of reservoirs, *SPE Annual Technical Conference and Exhibition* (1997).
13. Hillis, R.R., Pore pressure/stress coupling and its implications for seismicity, *Exploration Geophysics*, 31(2), 448-454 (2000).
14. Hillis, RR., Coupled changes in pore pressure and stress in oil fields and sedimentary basins, *Petroleum Geoscience*, 7(4), 419-425 (2001).
15. Hawkes, C.D., McLellan, P., and Bachu, S., Geomechanical factors affecting geological storage of CO_2 in depleted oil and gas reservoirs, *Journal of Canadian Petroleum Technology*, 44 (2005).
16. Rutqvist, J., Birkholzer, J., and Tsang, C-F., Coupled reservoir–geomechanical analysis of the potential for tensile and shear failure associated with CO_2 injection in multilayered reservoir–caprock systems, *International Journal of Rock Mechanics and Mining Sciences*, 45(2), 132-143 (2008).

7. Acknowledgements

This work was funded by the Gulf Coast Carbon Center at the Bureau of Economic Geology (BEG) and the U.S. Department of Energy, NETL, under contract numbers DE-FE0009301 and DE-FC26-05NT42590.